PHOTOCATALYTIC DEGRADATION OF PHENOL IN WATER BY SILVER/TITANIUM DIOXIDE NANORODS COATED WITH AN ULTRATHIN MAGNESIUM OXIDE LAYER

A Thesis

by

TYLER ANDREW SCOTT

Submitted to the Office of Graduate and Professional Studies of
Texas A&M University
in partial fulfillment of the requirements for the degree of

MASTER OF SCIENCE

Chair of Committee,	Ying Li
Committee Members,	Xingmao Ma
	Hong Liang
Head of Department,	Andreas Polycarpou

December 2017

Major Subject: Mechanical Engineering

ABSTRACT

Phenol is one of the most widespread, toxic, and recalcitrant compounds commonly found in water sources. Due to its persistent nature, conventional wastewater treatment methods are not effective to remove or degrade phenol from water. In this work, a novel photocatalyst is developed to degrade phenol under simulated sunlight. The catalyst is composed of a 1D titanium dioxide (TiO_2) nanorod decorated with elemental silver (Ag) nanoparticles, coated in an ultrathin magnesium oxide (MgO) layer through an atomic layer deposition (ALD) method. The prepared catalyst was characterized by scanning electron microscopy (SEM), x-ray diffraction (XRD), and UV-vis diffuse reflectance spectroscopy (UV-Vis DRS). The solar light photocatalytic performance of the material was evaluated and correlated with the material properties. The Ag decoration promoted light absorption and transfer of photo-induced electron-hole pairs from within TiO_2 nanorods to the catalyst surface. The ultrathin MgO layer with a subnanometer thickness further increased the light absorption and inhibited surface charge recombination through a surface passivation effect, promoting phenol degradation. The photocatalytic reaction mechanism was investigated by the examination of hydroxyl and superoxide radical production in the photocatalytic system. The results from this work demonstrate a new strategy for fabricating efficient sunlight-driven photocatalysts for the degradation of persistent water contaminants.

DEDICATION

To the only Lord of Heaven and earth, at whose name the mountains quake, whose unending mercy, grace, and provision have carried me thus far. In Your presence I have found peace and sustenance, strength and fullness of life. "'The Lord is my portion' says my soul, 'Therefore I will hope in Him.'" – Lamentations 3:24

ACKNOWLEDGEMENTS

First, and above all, I thank God for bringing me to graduate school, the people He brought into my life during this time, and His steadfastness through it all.

I would like to thank my advisor Dr. Ying Li for his guidance through my studies, from undergraduate to graduate, and his feedback throughout the entire process. Likewise, I am grateful for Dr. Xingmao (Samuel) Ma and Dr. Hong Liang, for serving on my thesis committee and providing insightful feedback.

To my fellow labmates, thank you for teaching me how to work in a chemical lab, for taking the time to help be talk through my research ideas, questions, and problems, and for helping me learn chemistry. Without you all I would not be where I am today. Specifically, thank you to Dr. Huilei Zhao for her wealth of knowledge and willingness to teach me what she knew. Thank you to Wei for always having the literature references I was looking for, to Xuhui for the countless TOC tests you ran for me, and to Fuping and Xianmei for your tireless work ethic which encouraged me when I was weary.

Thank you to Nate, for all of the excellent free coffee, the late-night fermentation projects, and for helping me to remember that there is much more to life than school. Thank you to my family in Oasis, for welcoming me quickly and openly, making me laugh always, and for giving me community when I needed it most.

Last, but far from least, I thank my family for always supporting and believing in me, for loving me unconditionally, for long conversations and excellent listening, for praying me through school. I love y'all more than I can put to words.

CONTRIBUTORS AND FUNDING SOURCES

This work was supported by a dissertation committee consisting of Professor Ying Li and Hong Liang of the Department of Mechanical Engineering, and Professor Xingmao Ma of the Department of Civil Engineering.

Scanning Electron Microscopy characterization was performed by Wei Deng, Photoluminescence and UV-Vis Diffuse Reflectance testing was conducted by Dr. Huilei Zhao, and Total Organic Carbon testing was performed by Xuhui Feng. All other work conducted for the dissertation was completed by the student independently.

Graduate study was supported by the Qatar National Research Fund

NOMENCLATURE

AOP	Advanced Oxidation Process
ALD	Atomic Layer Deposition
DI	De-Ionized
HPLC	High Performance Liquid Chromatography
TOC	Total Organic Carbon
SEM	Scanning Electron Microscopy
XRD	X-ray Diffraction
CB	Conduction Band
VB	Valence Band
ALD	Atomic Layer Deposition
SPR	Surface Plasmon Resonance
LSPR	Localized Surface Plasmon Resonance

TABLE OF CONTENTS

Page

LIST OF FIGURES

Page

LIST OF TABLES

Page

1. INTRODUCTION

1.1 Background

Globally, the need for clean water is high, and innovative solutions are needed to meet this growing demand as available water sources dwindle with increasing industrialization. Existing water sources are polluted by agricultural and industrial runoff from fertilizers, pesticides, plastics, pharmaceuticals, and other manufacturing processes. Many of these compounds are persistent in nature, and existing wastewater treatment methods such as biodegradation and adsorption are ineffective to completely remove them from water sources. In addition, existing treatment methods are often energy intensive, requiring the use of non-renewable fossil fuels. As global growth continues, it is necessary to utilize renewable energy resources such as solar energy. Thus, new, innovative, and renewable techniques are needed to address this complex problem.

Solar energy may be used for water treatment by heterogeneous photocatalytic degradation, where chemical pollutants are directly broken down by chemical reactions catalyzed by light activated semiconductors. This study focuses on the use and modification of these materials for the degradation of persistent organic chemicals.

1.2 Basics of Photocatalysis

Photocatalysis is defined as the acceleration of a photo-chemical reaction by a catalytic material. Photocatalysis garnered public attention through the work of Fujishima and Honda, who successfully split water through the use of TiO_2 as a semiconductor (Fujishima and Honda, 1972).

https://chriskresser.com/naturally-get-rid-of-acne-by-fixing-your-gut/ In typical semiconductor based photocatalytic reactions, the material absorbs an incident photon with energy greater than the materials band gap, E_g, leading to the excitation of an electron from the valence band to the conduction band of the material. When the excited electron is produced, it leaves behind a positively charged, and these free charge carriers may participate in the following reactions: 1.) oxidation of surface adsorbed compounds by holes, 2.) reduction of surface adsorbed compounds by electrons, 3.) volume recombination of electron-hole pairs, or 4.) surface recombination of electron-hole pairs (Linsebigler et al., 1995).

1.3 Fundamentals of Oxidative Degradation

Advanced oxidation processes (AOPs) are a set of chemical reactions used to degrade and remove various organic compounds in wastewater treatment. Typically, these reactions involve the use of oxidizing agents such as O_3, H_2O_2, and UV light to produce highly reactive hydroxyl ($^{\bullet}OH$) radicals, which are able to degrade the desired pollutants. $^{\bullet}OH$ radicals readily react with almost all organic compounds, and are able to oxidize nearly all of them as a result of their high oxidation potential, shown in Table 1 (Munter, 2001). Compared to ozone, a well-known and powerful oxidant, $^{\bullet}OH$ has higher reaction rates for many organic compounds, shown in Table 2 (Munter, 2001).

Table 1: Relative oxidation power of some oxidizing species. Reprinted from (Munter, 2001)

Oxidizing species	Relative oxidation power
Chlorine	1.00
Hypochlorous acid	1.10
Permanganate	1.24
Hydrogen peroxide	1.31
Ozone	1.52
Atomic oxygen	1.78
Hydroxyl radical	2.05
Positively charged hole on titanium dioxide, TiO_2^+	2.35

Table 2: Reaction rate constants (k, M^{-1} s^{-1}) of ozone vs $^{\bullet}OH$ radical. Reprinted from (Munter, 2001)

Compound	O_3	$^{\bullet}OH$
Chlorinated alkenes	10^3–10^4	10^9–10^{11}
Phenols	10^3	10^9–10^{10}
N-containing organics	10–10^2	10^8–10^{10}
Aromatics	1–10^2	10^8–10^{10}
Ketones	1	10^9–10^{10}
Alcohols	10^{-2}–1	10^8–10^9

In general, the hydroxyl radical attacks the target compound through either the abstraction of a hydrogen atom, or through the hydroxylation of the molecule by attaching itself to the contaminant. Mineralization, the decomposition of compounds into soluble inorganic forms, is readily achieved for many chemicals when attacked by the hydroxyl radical. In this process, chlorinated compounds often form several intermediates, and finally CO_2, H_2O, and chloride ions. Sulphur containing compounds form sulphate, and nitrogen containing compounds form N_2 or nitrate. As such, AOPs

are a powerful tool for water treatment, able to potentially reduce pollutant concentrations from several hundred ppm to single ppb levels (Munter, 2001).

Many methods exist to produce •OH for AOPs, both photo-chemical and non-photochemical. All of these methods include oxidizing agents such as O_3, H_2O_2, and UV light, sometimes combined with catalysts to enhance the reaction rates.

1.3.1 Non-photochemical Methods

Among the non-photochemical methods, the most popular are the pairing of O_3 with a catalyst, and the Fenton system of H_2O_2 with Fe^{2+}. In the O_3/catalyst system, various metal oxides and ions such as Fe_2O_3, Al_2O_3, TiO_2, Fe^{2+}, and Fe^{3+} have been used as catalysts. In many cases, the addition of the catalyst to the system markedly increases the efficiency of TOC reduction in wastewater, though this performance enhancement is dependent on the catalyst. Cortés et al. found that O_3/Mn(II) and O_3/Fe(II) systems were more effective than O_3/high pH or O_3/Fe(III) systems for the degradation of chlorobenzenes in wastewater (Cortés et al., 2000). Under acidic pH conditions, the addition of alumina to ozone increased the TOC degradation of 2-chlorophenol by 83.7% (Kasprzyk-Hordern et al., 2003). Beltrán et al. found that the addition of transition metal oxides, Fe, Ti, and Co, when supported on alumina, increased the TOC degradation of ozonated phenol. For all catalysts, the consumption of ozone per mg of mineralized compound was reduced as compared to the non-catalyzed reaction, in some cases as high as a 50% reduction. Among the three metals tested, Co yielded the greatest improvement (Beltrán et al., 2003).

In the Fenton system, hydroxyl radicals are produced through the reduction of Fe^{2+} to Fe^{3+} according to Equation 1.1.

$$Fe^{2+} + H_2O_2 \rightarrow Fe^{3+} + OH^- + {}^{\bullet}OH \quad (1.1)$$

The Fenton system is well studied, and has been shown to be effective for the degradation of many compounds including nitrophenols, pharmaceutical effluent, and herbicides (Lipczynska-Kochany, 1991; Tekin et al., 2006; Trapido et al., 1998; Upelaar et al., 2000). In all cases, the active species is the hydroxyl radical, and the reaction rate is highly dependent on pH, performing best in acidic solutions. In addition, the Fenton system is attractive for wastewater treatment because iron is abundant and non-toxic, and hydrogen peroxide is relatively low cost and benign. However, the iron requirement is somewhat high, as the molar ratio of produced ˙OH to required iron is 1:1, thus requiring a large amount of Fe for treatment.

1.3.2 Photochemical Methods

In many of the photochemical methods, UV irradiation is used in addition to the oxidizing agents, and in photo-Fenton and photocatalytic oxidation systems, catalytic materials are added to further increase the rate of reaction. In systems utilizing only the oxidizing agents without the addition of UV irradiation, degradation of the target compounds is often incomplete, converting the original species into intermediate compounds which may be more reactive and toxic (Scheck and Frimmel, 1995).

In the UV/O_3 system, O_3 reacts with H_2O to form H_2O_2, which may then photodecompose into ˙OH or react with O_3 to form ˙OH. The overall reaction equation is shown below in Equation 1.2.

$$O_3 + h\nu + H_2O \rightarrow 2^{\bullet}OH + 3O_2 \quad (1.2)$$

Irmak et al. found that for the degradation of 17ß-estradiol (E_2), as compared to oxidation by O_3 alone, for the same degradation amount, the coupling of UV/O_3 reduced the O_3 demand by 22.5%, and reached the same level of degradation in less time (Irmak et al., 2005). Peyton and Glaze studied the reaction mechanism of O_3 photolysis and determined that aqueous O_3 reacts to form H_2O_2, which further reacts to form $^{\bullet}$OH, which serves as the primary reactive species (Peyton and Glaze, 1988).

The irradiation of H_2O_2 with UV leads directly to the formation of $^{\bullet}$OH radicals, according to Equation 1.3, with a quantum yield of two hydroxyl radical per absorbed photon.

$$H_2O_2 + h\nu \rightarrow 2^{\bullet}OH \quad (1.3)$$

Elkanzi and Kheng investigated the degradation of isoprene using various molar ratios of H_2O_2 to isoprene, finding that increasing the relative amount of H_2O_2 increases the degradation rate linearly. In addition, the amount of H_2O_2 was found to be relatively constant with time, which is explained by the reaction of the hydroxyl radical with hydrogen peroxide to form the hydroperoxyl radical, which is able to regenerate hydrogen peroxide; this claim is supported by the findings of other groups (Benitez et al., 1996; Elkanzi and Bee Kheng, 2000)

The photo-Fenton system is identical to the UV/H_2O_2 system, but with the addition of Fe^{3+} ions. In this system, $^{\bullet}$OH are produced from the photolysis of H_2O_2, the reduction of Fe^{3+} to Fe^{2+} according to Equation 1.4, and the reaction of Fe^{2+} with H_2O_2 according to Equation 1.1.

$$Fe^{3+} + H_2O + h\nu \rightarrow Fe^{2+} + H^+ + {}^{\bullet}OH \quad (1.4)$$

In this way, additional ·OH is generated as compared to a typical Fenton-system, increasing the total degradation activity. Although hydrogen peroxide has low light absorption in the visible spectra, the absorbance of the ferric ion extends to the near-UV/visible region, enabling the photo-Fenton system to operate under visible light conditions. While many AOPs, including the standard Fenton system, are able to fully degrade chemical compounds, mineralization is often incomplete. Photo-Fenton systems exhibit high mineralization performance for a variety of organic pollutants. Leónidas et al. reported the complete mineralization of a 50 ppm diclofenac solution in 100 minutes, with complete degradation in 60 minutes (Pérez-Estrada et al., 2005). Wu et al. reported that in the dark, a typical Fenton system mineralized only 6% of a Malachite Green dye solution after 90 minutes, however under visible irradiation, 100% mineralization was achieved after 160 minutes (Wu et al., 1999).

In solid semiconductor based photocatalytic oxidation, incident light, often UV, supplies energy to excite an electron to the conduction band of the material, leaving a positively charged hole in the valence band. These photogenerated carriers are able to participate in either reduction or oxidation reactions (Matthews, 1986):

$$e^- + O_2 \rightarrow {}^{\bullet}O_2^- \quad (1.5)$$

$$h^+ + A^- \rightarrow {}^{\bullet}A \quad (1.6)$$

$$h^+ + OH^- \rightarrow {}^{\bullet}OH \quad (1.7)$$

$${}^{\bullet}OH + RH \rightarrow {}^{\bullet}OHRH \quad (1.8)$$

$${}^{\bullet}OH + RH \rightarrow {}^{\bullet}R + H_2O \quad (1.9)$$

$$h^+ + RH \rightarrow {}^{\bullet}RH^+ \quad (1.10)$$

Photogenerated holes have a high oxidation potential and are thus able to oxidize almost any chemical compound. Their oxidation potential is great enough such that the one-electron oxidation of water, forming the hydroxyl radical, should be feasible:

$$H_2O + h^+ \rightarrow {}^{\bullet}OH + H^+ \quad (1.11)$$

Common semiconductors for this process include zinc oxide (ZnO), titanium dioxide (TiO_2), iron oxide (Fe_2O_3), and cadmium sulfide (CdS) (Yasmina et al., 2014). Among these, TiO_2 is an attractive material as it is non-toxic, photo-stable, low-cost, and abundant. Frank and Bard were the first to report the use of TiO_2 for the photocatalytic oxidation of CN^- and SO_3^{2-} under sunlight (Frank and Bard, 1977). Since then, TiO_2 has been thoroughly studied for the degradation of many compounds, under many different testing conditions.

1.4 TiO_2 Based Photodegradation

1.4.1 Properties of TiO2

TiO_2 exists in either an amorphous phase, or in one of its three crystalline phases, anatase, rutile, and brookite. Rutile and anatase are the phases most commonly used in photocatalysis, however some groups have reported the use of an anatase rich brookite mixture with higher photocatalytic activity than anatase alone (Liu et al., 2013). Anatase is often reported to be the most photocatalytically active, however rutile is more thermodynamically stable; anatase will transform to rutile if heated above ~600-700°C (Rajeshwar et al., 2001). The crystal lattice of both anatase and rutile is composed of chains of TiO_6 octahedra, but with different arrangements. In rutile, the two edges

connect the octahedral with their nearest neighbors, while in anatase the lattice octahedrals share four edges. The structures of anatase and rutile are shown below in Figure 1 (Verbruggen, 2015).

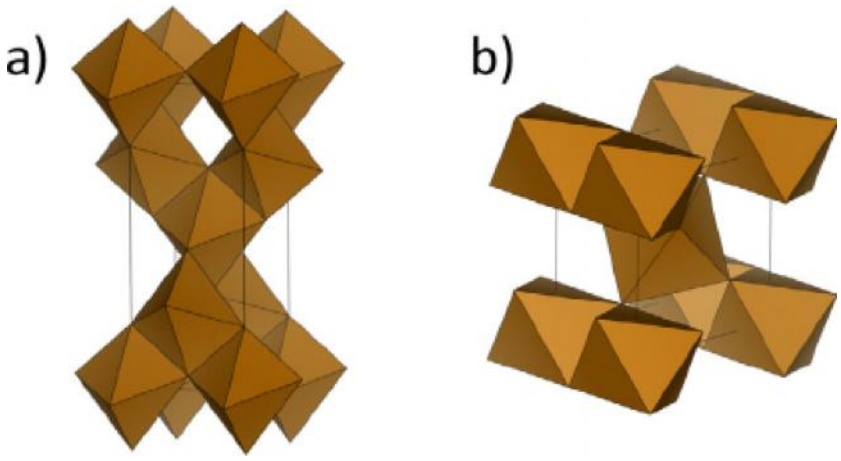

Figure 1: Three-dimensional crystal structure representation of the TiO_6 octahedral in (a) anatase and (b) rutile. Reprinted from (Verbruggen, 2015).

The different crystal structures of anatase and rutile result in different band gaps, 3.2 eV for anatase, and 3.0 eV for rutile (Habisreutinger et al., 2013).

1.4.2 Challenges and Approaches

In spite of its many advantages, TiO_2 has some drawbacks which may hinder its efficacy for photocatalytic degradation. The large band gap of anatase requires high energy photons to promote electrons, and this energy corresponds to light of wavelength less than 380 nm, in the UV region. Less than 10% of the solar spectrum is composed of UV light, thus TiO_2 has low activity for solar and visible light applications (Linsebigler

et al., 1995). In addition, the photonic efficiency of TiO_2 is relatively low, less than 10% as reported by Schneider et al., and this results from a high recombination rate of the photogenerated charge carriers (Herrmann, 1999; Schneider et al., 2014). These two factors, low visible light absorption and a high charge recombination rate, hinder the performance of TiO_2, and thus many efforts have been made to overcome them.

1.4.2.1 Physical Structure

One of the most common structures of TiO_2 is nanoparticles. The small size of these particles results in a large specific surface area, making them highly effective for photocatalytic reactions because more surface sites are available to participate in oxidation and reduction reactions at any given time. However, their small size also results in expensive and difficult recapture. If the small particles are not completely recollected after degradation, the particles become a pollutant in themselves. To address this implementation issue, different physical structures and immobilization techniques have been used to increase the ease of recapture or eliminate the need for it entirely. Thin films of TiO_2 have the advantage of enabling different operational modes, as there is no need for recollection. As such, these films may be easily implemented into continuous treatment systems. However, these thin films typically have reduced surface area as compared to nanoparticles, resulting in reduced catalytic efficiency. Some groups, however, have reported increased performance in thin films. Sopyan et al. reported that a thin TiO_2 film prepared by sol sintering was more effective for the degradation of gaseous acetaldehyde than the standard benchmark, Degussa P25 particles. This was attributed to an increase in the number of surface adsorption sites per

unit true surface area, coupled with increased charge separation resulting from the film geometry (Sopyan et al., 1996).

One dimensional (1D) structures such as nanotubes, nanowires, and nanofibers have risen in popularity because of several inherent advantages. Their 1D geometry allows for fast and long-distance transfer of electrons, reducing charge recombination. The high length-to-diameter ratio of these materials results in increased light absorption as compared to nanoparticles, and the overall increase in structure size allows for ease of recollection (Xiao et al., 2015; Yuan and Su, 2004).

1.4.2.2 Addition of Noble Metals

The addition of noble metals such as platinum (Pt), gold (Au), and silver (Ag) to TiO_2 has been used to enhance its catalytic performance by reducing electron-hole recombination (Buso et al., 2007; Choi et al., 1994; Kubacka et al., 2008; Tian and Tatsuma, 2004) and increasing light absorption through localized surface plasmon resonance, wherein the collective oscillation of surface electrons increases UV-Vis light absorption (Tian and Tatsuma, 2004). Among these metals, Ag has shown particularly high performance for enhancing photocatalytic activity, and additionally, it has a relatively low cost, is naturally abundant, and is easy to implement (Cozzoli et al., 2004). Cui et al. found that the addition of Ag and Ag_2O particles to reduced TiO_2 increased the light absorption in a broad region from 400-800 nm, and exhibited a higher charge separation efficiency, resulting in increased degradation of diclofenac under visible light irradiation (Cui et al., 2017). In addition to its photocatalytic properties, Ag nanoparticles have potent antibacterial activity, making them especially valuable for

water treatment (Kubacka et al., 2008; Li et al., 2008). Liu et al. reported that a Ag/TiO_2 nanofiber membrane was able to degrade methylene blue more effectively than a TiO_2 only membrane, and that the addition of the Ag lent antibacterial properties, reducing biofouling (Liu et al., 2012).

1.4.2.3 Thin Metal Oxide Coatings

Recently, thin metal oxide layers including zirconium dioxide (ZrO_2), aluminum oxide (Al_2O_3), tin oxide (SnO_2), and magnesium oxide (MgO) have been used to reduce the recombination rate of generated electron-hole pairs in organic photovoltaics and TiO_2, to enhance the photoluminescence of ZnO nanowires, and to act as protective coating in various optoelectronics (Le Formal et al., 2011; Li et al., 2009; Song et al., 2014; Xi et al., 2013; Zhao et al., 2017). Song et al. found that a thin MgO layer grown using plasma enhanced atomic layer deposition (PE-ALD) was effective to passivate the surface of ZnO nanowires (Song et al., 2014). Very recently, Zhao et al. reported that the addition of a thin Al_2O_3 layer to the surface of reduced anatase nanorods increased CO_2 photoreduction yields by passivating existing surface states, reducing electron-hole recombination (Zhao et al., 2017). In these catalysts, the coating uniformity and thickness were critical in obtaining the desired results, having an optimum coating thickness at which performance was enhanced. Thus, these ultrathin layers were grown using ALD, which utilizes self-limiting surface reactions to create highly uniform and conformal coatings of controllable thickness. Each cycle of ALD consists of the sequential reaction of at least two chemical precursors to form a new layer of the desired material, with subnanometer thicknesses achievable (Aarik et al., 2001).

2. OBJECTIVES

The specific objectives of this study are:

1. To investigate the potential performance enhancement of an ultrathin MgO coating on Ag decorated TiO_2 nanorods.
2. To investigate the specific reaction mechanism by which the MgO layer enhances or alters the photocatalytic performance.

The decoration of Ag nanoparticles may enhance visible light absorption while reducing electron-hole recombination, and the addition of the MgO layer may further increase performance by passivating surface traps on TiO_2. While thin metal oxide layers have been used in the areas of dye sensitized solar cells (DSSC) and CO_2 photoreduction, their application in aqueous photocatalytic oxidation reactions is mostly unexplored. The produced catalyst will be studied in terms of its physical properties and crystalline structure, as well as its optical properties. Its photocatalytic performance will be evaluated by the photooxidation of phenol under solar irradiation. The reaction mechanisms will be investigated by the examination of hydroxyl and superoxide radical production in the photocatalytic system.

3. MATERIALS AND METHODS

3.1 Materials

Titanium dioxide (P25 powder) was purchased from Evonik. Sodium hydroxide (NaOH), hydrochloric acid (HCl, 37%), ethanol (97%), and methanol (99.8%) were purchased from Fisher Scientific. Silver nitrate ($AgNO_3$) and crystalline phenol (99%) were purchased from SigmaAldrich. Bis(ethylcyclopentadienyl)magnesium (98%), tetrakis(dimethylamino)titanium (99%), and trimethylaluminum (98%) were purchased from Strem Chemicals.

3.2 Material Synthesis

3.2.1 Synthesis of TiO_2 Nanorods

TiO_2 nanorods were produced using a simple hydrothermal process. First, 2.0 g of P25 was added to 160 ml 10M NaOH and stirred overnight. The resulting mixture was sealed in a 200 ml Teflon-lined autoclave, and heated in an electric furnace at 180°C for 48 h, with a ramp rate of 8°C/min. Next, the obtained nanorods were washed alternately with 0.1 M HCl and deionized (DI) water until pH 7; they were then dried overnight at 60°C and calcined at 450°C for 2 h to obtain TiO_2 nanorods.

3.2.2 Synthesis of Ag_TiO_2 Nanorods

Ag nanoparticles were decorated on the surface of TiO_2 nanorods using a simple ultraviolet (UV) deposition method. Briefly, 50 mg of TiO_2 nanorods was added to a solution of 15.75 mg $AgNO_3$, 5 ml DI water, and 0.2 ml ethanol, and sonicated for 10 minutes to obtain a homogeneous mixture. This mixture was then irradiated for 2 h using

a 100 W UV lamp (UVP Blak-Ray B-100AP) under constant stirring. After thorough washing with DI water and overnight drying at 60°C, Ag_TiO_2 were obtained, with a theoretical 5% mass loading of Ag.

3.2.3 Synthesis of MgO@Ag_TiO_2 Nanorods

To coat Ag_TiO_2 with a thin layer of MgO, ALD (Savannah S200, Ultratech) was used. For each sample, Ag TiO_2 was loaded in a homemade particle holder and placed in the center of the reaction chamber. To ensure a uniform coating, "expo mode" was used, in which the reactor is sealed while the precursors react with the sample, to increase surface contact time. The pulse time for both H_2O and MgO precursor was 2 seconds, the magnesium cylinder was maintained at 95°C, and the reactor was maintained at 200°C. The obtained catalyst was denoted X_MgO@Ag_TiO_2, where X is the number of ALD cycles.

3.3 Characterization of Prepared Catalysts

Scanning electron microscopy (SEM) analysis was performed using a JEOL JSM7500F instrument. X-ray diffraction (XRD) analysis was performed using a BRIKER D8 system, with Cu Kα irradiation at 45 kV and 40 mA. UV-vis diffuse reflectance spectra (DRS) were obtained with a Hitachi U4100 UV-vis-NIR spectrophotometer.

3.4 Photocatalytic Activity Testing

The activity of the prepared catalysts was evaluated by the photodegradation of phenol under simulated solar irradiation provided by a 150 W Oriel® Sol1A system (Newport Inc.). For each test, 10 mg of catalyst was added to a 50 ml solution of 15

mg/L phenol, sonicated for 10 minutes to uniformly disperse the catalyst, and irradiated. At 30 minute intervals, 0.5 ml samples were taken and filtered using a 0.45 µm PTFE syringe filter to remove the catalyst. The obtained solutions were analyzed using a Shimadzu 2030C high performance liquid chromatography (HPLC) equipped with a Phenomex 5 µm C18 00F-4601 (150 x 4.6 mm) column with a fixed detection wavelength of 254 nm. The mobile phase was a mixture of acetonitrile and DI water with a varying volume mixture and constant flow rate of 1 ml min^{-1}. In order to determine the level of mineralization, the total organic carbon (TOC) of each sample was measured using a Shimadzu TOC-V WP.

4. RESULTS AND DISCUSSION

4.1 Morphology, Crystal Structure, and Optical Properties

To observe the structural transformation of the TiO_2 from nanoparticles to nanorods, SEM was performed. P25 has an average diameter of 21 nm, and is composed of approximately 80% anatase and 20% rutile. In Figure 2, the produced nanorods have an average diameter of 100 nm, with a length of 1-2 μm. These dimensions confirm the desired 1D structure of the nanorods, and this increased size results in easy recollection of the catalyst.

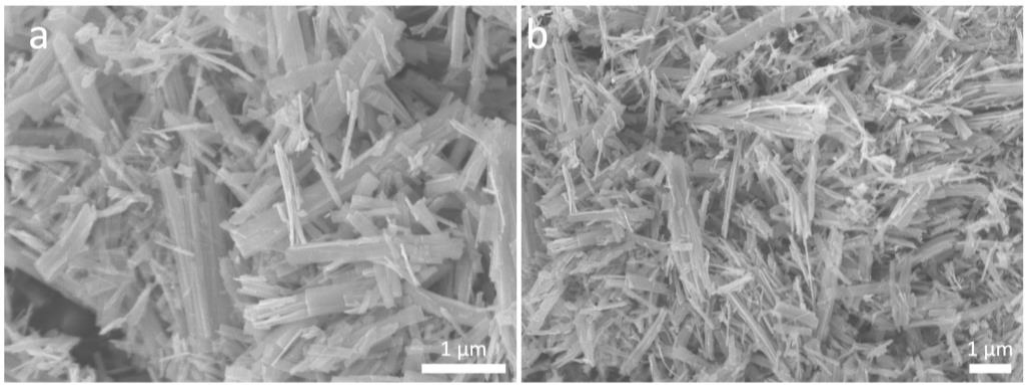

Figure 2: Geometry of synthesized TiO_2 nanorods

XRD analysis was conducted to investigate the crystal structure of Ag_TiO_2; the spectrum of TiO_2 was measured as a reference. Shown in Figure 3, the spectrum of TiO_2 contains characteristic peaks at 25° and 48°, corresponding to the (101) and (200) facets for anatase (JCPDS 21-1272). In addition, peaks at 28.8°, 44°, and 58° correspond to hydrogen titanate impurities (Kataoka et al., 2013). The spectrum of Ag_TiO_2 contains

an additional peak at 38°, which corresponds to the (111) plane of metallic silver (JCPDS 01-0783).

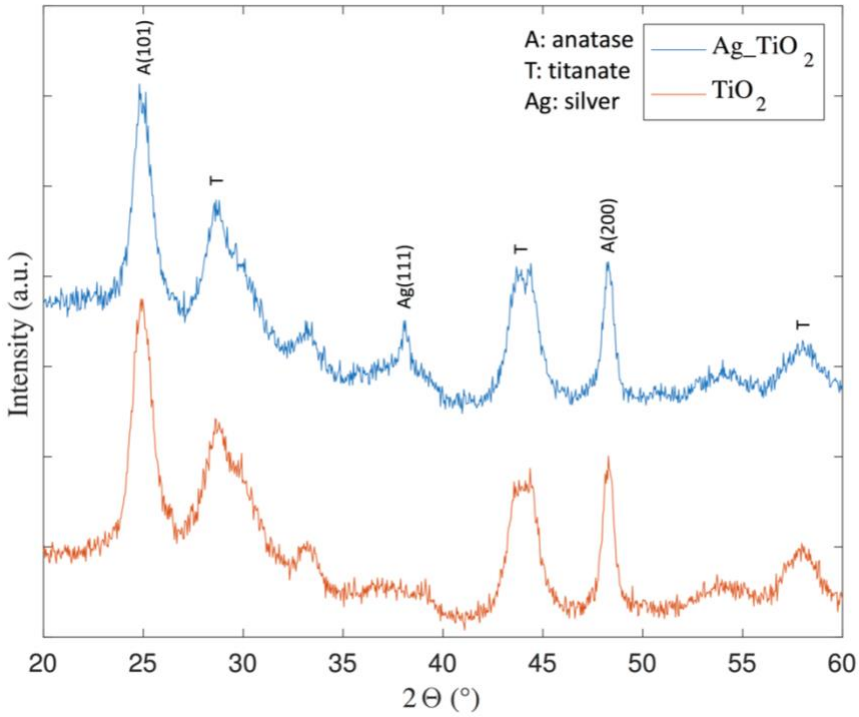

Figure 3: XRD Spectrum of TiO_2 and Ag_TiO_2

The optical properties of the produced catalysts were characterized by UV-Vis DRS and Tauc analysis. From Figure 4a, in agreement with literature, the addition of Ag particles to TiO_2 increases the light absorption in both the UV and visible regions as a result of surface plasmon absorption, with a peak in the visible region at 517 nm (Cui et al., 2017; Liu et al., 2012; Yu et al., 2005). The large red-shift of this peak compared to the commonly reported Ag plasmon peak at 400 nm may be associated with the relatively high refractive index of TiO_2 as well increased Ag particle size, which is correlated with

red-shifted plasmonic peaks (Lee et al., 2008; Tian and Tatsuma, 2004). The addition of the ultrathin MgO layer further increases the light absorbance in both the UV and visible regions, while the visible absorbance peak is shifted to 504 nm and decreases in intensity. Hore et al reported that the addition of a thin ZrO_2 layer atop a TiO_2 layer increased the efficiency of a dye sensitized solar cell (DSSC) due to enhanced light scattering, and that this scattering is dependent on the difference in refractive indices of the two materials (Hore et al., 2006). The difference in the refractive indices of MgO and TiO_2 is greater than that of ZrO_2 and TiO_2, therefore it is likely that the addition of the ultrathin MgO layer increased light absorption by enhancing light scattering and reducing reflection. In both Ag_TiO_2 and 5_MgO@Ag_TiO_2, the additional light absorption will increase the generation of photogenerated electron-hole pairs that participate in photocatalytic reactions. From the produced Tauc plot in Figure 4b, the bandgap was calculated to be 3.18 eV for all three catalysts. The additions of the Ag NPs and MgO layer do not affect the crystal structure of the nanorods, because if the Ag or MgO had been doped into the surface lattice, a reduction in bandgap would be expected (Li et al., 2016).

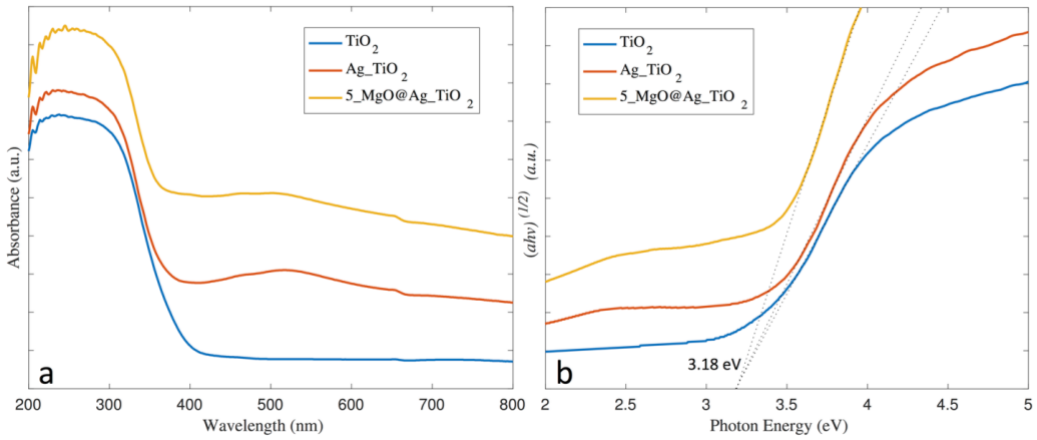

Figure 4: (a) UV-Vis Diffuse-reflectance spectra and (b) Tauc plot for TiO_2, Ag_TiO_2, and $5\_MgO@Ag\_TiO_2$

4.2 Photocatalytic Performance

To determine the photocatalytic activity of the synthesized catalysts, phenol was used as a probe pollutant and tested for degradation under solar irradiation. First, the irradiation time for Ag deposition was varied to alter the amount and size of the deposited Ag particles (Piwoński et al., 2016). Two hours was the optimum irradiation time; shorter and longer irradiation times, 1, 2.5, and 3 hours decreased performance, as shown in Figure A1. For shorter irradiation times, fewer and smaller particles may be deposited on the nanorods; the reduced amount of Ag may not be able to trap enough electrons to significantly impact charge recombination rates. For longer irradiation times, the total amount of deposited Ag is likely unchanged, but with fewer and larger particles due to aggregation (Piwoński et al., 2016). When the small particles aggregate into larger clumps, the dispersion uniformity of the particles is decreased, which may cause an increase in the charge recombination rate as compared to the optimum Ag loading. In

addition to changes in charge recombination rates, the physical properties of the deposited nanoparticles will affect the light absorption effect displayed in the DRS results, both peak wavelength and intensity (Kelly and Johnston, 2011).

Coating thin layers of various metal oxides has been shown to benefit catalyst performance by enhancing charge separation through surface trap passivation (Mali et al., 2015; Song et al., 2014; Vasilopoulou et al., 2014). Therefore, thin coatings of TiO_2, Al_2O_3, and MgO were deposited on Ag_TiO_2. Figure A2 shows that one cycle of either TiO_2 or Al_2O_3 significantly decreases performance, whereas one cycle of MgO has a neutral effect, not significantly changing the performance of the catalyst. Additional cycles of both TiO_2 and Al_2O_3 were tested and found to decrease performance. The decrease in performance due to the TiO_2 and Al_2O_3 layers is attributed to hindered electron-hole mobility, and thus an increased recombination rate. Following the mixed result of one MgO cycle, additional cycles of MgO were tested.

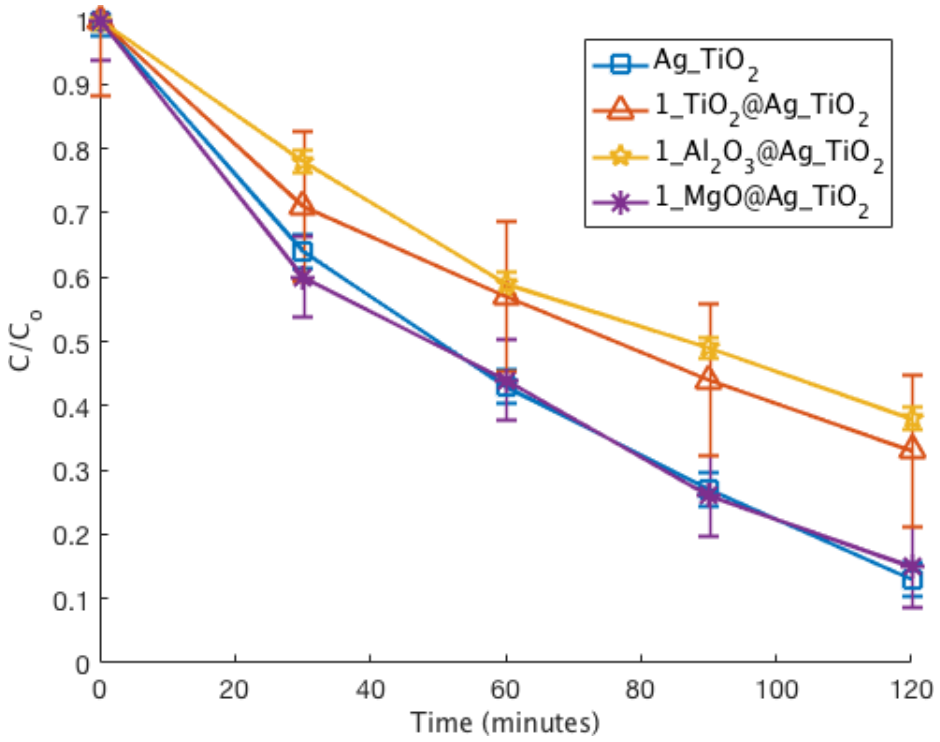

Figure 5: Effect of metal oxide coating material on 120 min degradation of 50 ml 15 ppm phenol solution with 0.2 g/L catalyst loading under solar irradiation

As shown in Figure A2, depending on the number of cycles, the performance may be enhanced or hindered. A coating of 5 cycles increases performance, achieving 95% degradation of phenol in 120 min. The thin layer of MgO is able to passivate existing surface traps and thus reduce electron-hole recombination rates, increasing photocatalytic activity. However, due to the thin nature of the deposited layer, the electron remains able to travel to the surface of the catalyst and react with chemical molecules to degrade phenol (Bandara and Pradeep, 2008). Increasingly thick layers beyond 5 cycles decrease performance, with 10 cycles performing slightly better than

Ag_TiO_2, and 20 cycles performing worse. These thick layers may inhibit photocatalytic activity by the amount of surface electrons available for chemical reactions.

Figure 6 shows that 5_MgO@Ag_TiO_2 degrades 95% of phenol in 120 min, Ag_TiO_2 degrades 87%, and TiO_2 degrades 75%. Comparing the kinetics of each catalyst based on pseudo first-order kinetics from the Langmuir-Hinshelwood model, rate constants were found to be 0.01124, 0.01648, and 0.02505 min^{-1} for TiO_2, Ag_TiO_2, and 5_MgO@Ag_TiO_2 respectively. From these results, the addition of Ag nanoparticles increased the degradation rate constant of TiO_2 by 46.6%, and the addition of the ultrathin MgO layer increases the degradation rate constant of $AgTiO_2$ by 52%.

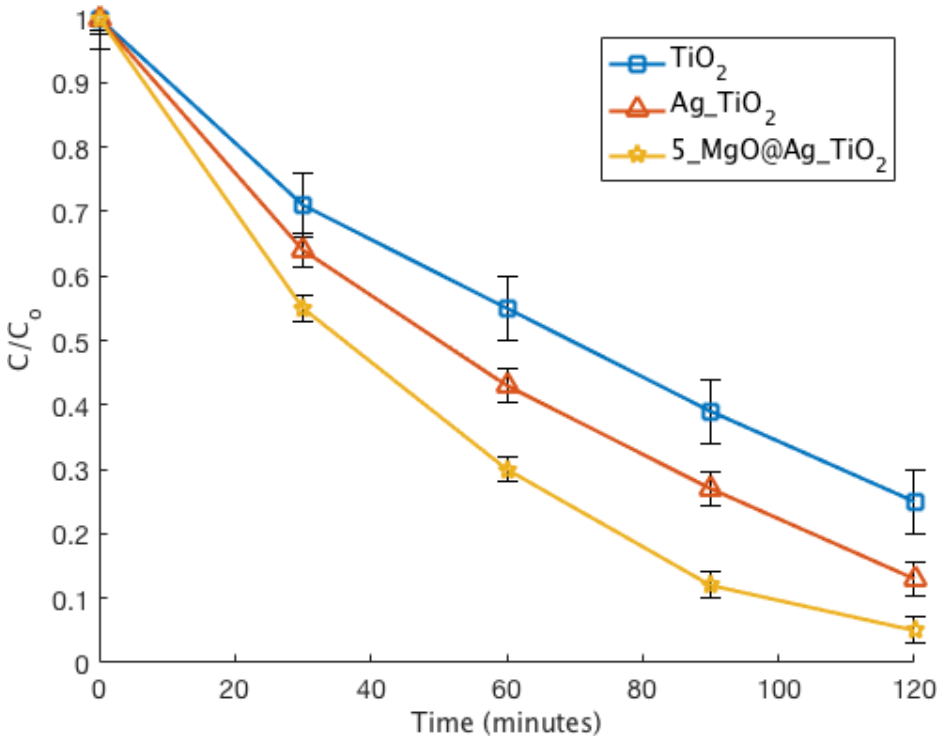

Figure 6: TiO_2, Ag_TiO_2, and 5_MgO@Ag_TiO_2 120 min degradation of 50 ml 15 ppm phenol solution

TOC analysis was conducted to determine the mineralization performance of each catalyst. Results show that TiO_2, Ag_TiO_2, and 5_MgO@Ag_TiO_2 mineralize 42%, 54%, and 24% respectively of the initial phenol solution after 120 min solar irradiation, shown in Figure 7. The addition of Ag nanoparticles increases the performance mineralization performance, however the further addition of MgO decreases the performance by more than half, despite the improved degradation performance of 5_MgO@Ag_TiO_2. This is further evidenced by the HPLC spectra shown in Figures A4-7. After 120 minutes of irradiation, additional peaks, and of greater area, are seen in the 5_MgO@Ag_TiO_2 spectra that are not present for Ag_TiO_2. These likely indicate a

variety of phenol intermediates due to the lower mineralization performance of 5_MgO@Ag_TiO_2.

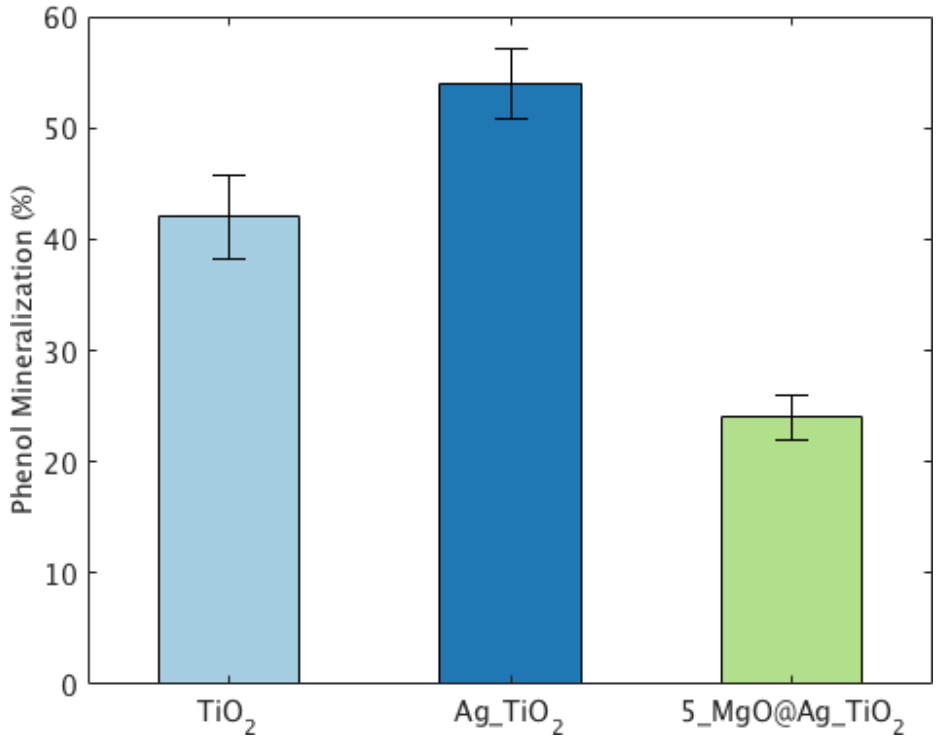

Figure 7:Phenol mineralization by TiO_2, Ag_TiO_2, and 5_MgO@Ag_TiO_2 of 50 ml 15 ppm phenol solution with 0.2 g/L catalyst loading after 120 min solar irradiation

4.3 Contribution of Reactive Species

To determine the influence of different reactive species in the degradation processes, several scavenging tests were performed. In each of these tests, a specific reactive species was scavenged by the addition of various chemicals to the phenol solution, and the effect on the photocatalytic performance was observed. All tests were performed under the same test conditions as photocatalytic performance, but for a duration of 60

minutes. First, ethylenediaminetetraacetic acid (EDTA) was added to scavenge generated holes (Ji et al., 2013). From Figure 8, Ag_TiO_2 experiences a modest decrease in performance, decreasing from 57% to 40% degradation, indicating that h^+ plays a role in degradation. In 5_MgO@Ag_TiO_2, the addition of EDTA decreases the performance to a larger degree, 70% to 38%, than in Ag_TiO_2, suggesting that h^+ is of increased importance. These photogenerated holes are able to react with H_2O to form •OH according to Equation 4.1, or they may directly oxidize phenol (Ilisz and Dombi, 1999).

$$h^+ + H_2O \rightarrow H^+ + \bullet OH \tag{4.1}$$

The influence of generated electrons was investigated by removing dissolved O_2 from the solution. This was accomplished by bubbling Argon for 30 minutes prior to testing, which was then carried out in an anaerobic cell. Argon purging significantly reduced the performance of both Ag_TiO_2, 57% to 26%, and 5_MgO@Ag_TiO_2, 70% to 15%, suggesting that the electron plays an important role in the degradation processes of both catalysts, perhaps greater than the hole, as the dissolved O_2 can act as an electron trap by forming $\bullet O_2^-$ according to Equation 4.2.

$$e^- + O_2 \rightarrow \bullet O_2^- \tag{4.2}$$

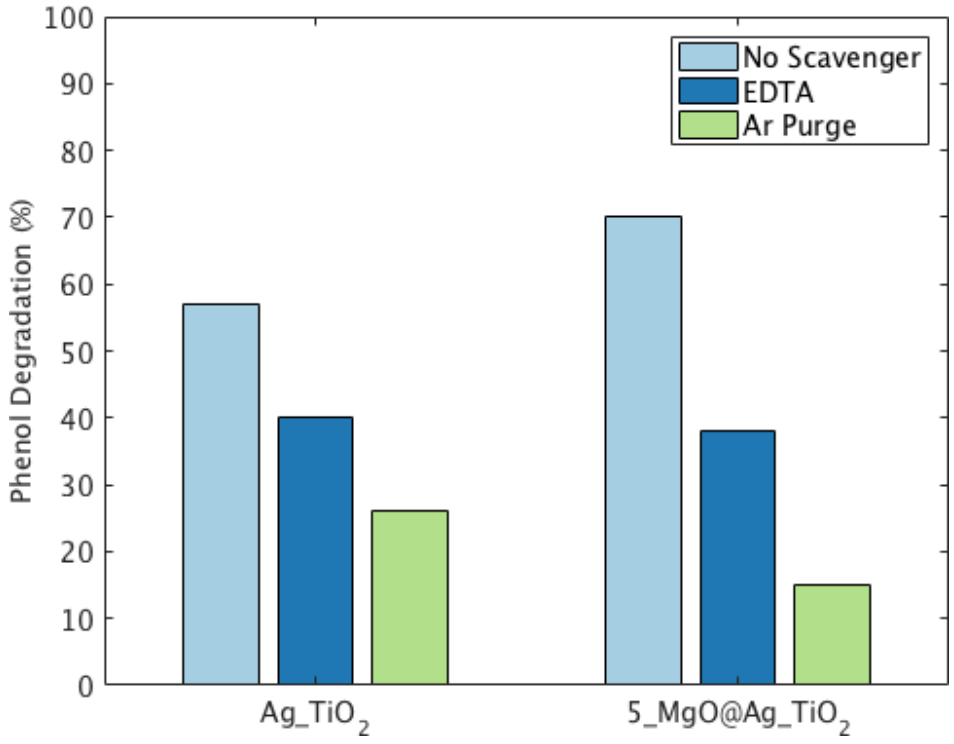

Figure 8: 60 min scavenger study results for Ag_TiO_2 and 5_MgO@Ag_TiO_2

To compare the production of •OH and •O_2^- in each catalyst, chemical probes were utilized. In solution, terepthalic acid (TA) reacts with •OH to form 2-hydroxyterepthalic acid (HTA), which, when exposed to UV light, fluoresces in the visible spectrum (Ishibashi et al., 2000). To measure •OH production, each catalyst was dispersed in a TA solution and irradiated for 60 minutes. Samples were taken every 15 minutes and measured using a PTI QuantaMaster series spectrofluorometer with UV irradiation at 315 nm and maximum absorbance at 429 nm. Figure 9 shows that the addition of Ag nanoparticles to the surface of TiO_2 increases •OH production, and that the further addition of the ultrathin MgO layer reduces •OH production to levels below that of TiO_2. The increase in •OH production by Ag_TiO_2 may result from the increased light

absorption, generating more electron-hole pairs, as well as the increased charge separation provided by the metallic particles acting as electron traps. In 5_MgO@Ag_TiO_2, the ultrathin layer may hinder hole mobility, which would reduce the number of holes available on the surface of the catalyst to form •OH.

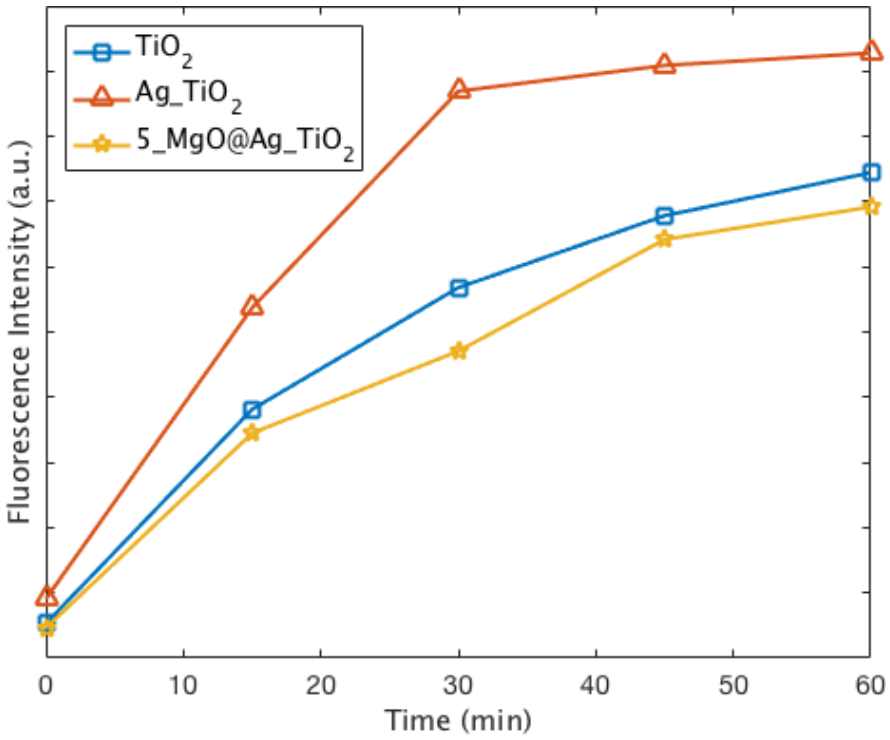

Figure 9: HTA fluorescence for TiO_2, Ag_TiO_2, and 5_MgO@Ag_TiO_2

The large performance drop induced by O_2 scavenging may arise from a lack of superoxide production, or an increase in electron-hole recombination. To investigate superoxide production for each catalyst, nitroblue tetrazolium (NBT) was used a probe. NBT reacts with $•O_2^-$ to form insoluble purple formazan, and has an absorption peak at 259 nm, which was measured using a UV-vis spectrophotometer (Shimadzu UV-2600)

(Xu et al., 2010). Similar to the TA test, each catalyst was dispersed in a weak NBT solution and irradiated, with samples taken every 15 minutes. Figure 10 shows that 5_MgO@Ag_TiO_2 reduces the most NBT of all three catalysts, and at the highest rate, indicating that it produces the most $\bullet O_2^-$. In fact, 5_MgO@Ag_TiO_2 reduces more NBT in 15 minutes than either of the other catalysts in 60 minutes. This increased production rate may be caused by a combination of the MgO layer increasing the total number of generated electron hole pairs through increased light absorption, and the passivation of surface traps, resulting in a reduced recombination rate of the generated electron-hole pairs. In addition, while the MgO layer likely does not hinder electron mobility due to its thin nature, it may hinder hole mobility, further reducing surface recombination. Combined, these effects could increase the number of electrons available on the catalyst surface to react with O_2 to form $\bullet O_2^-$.

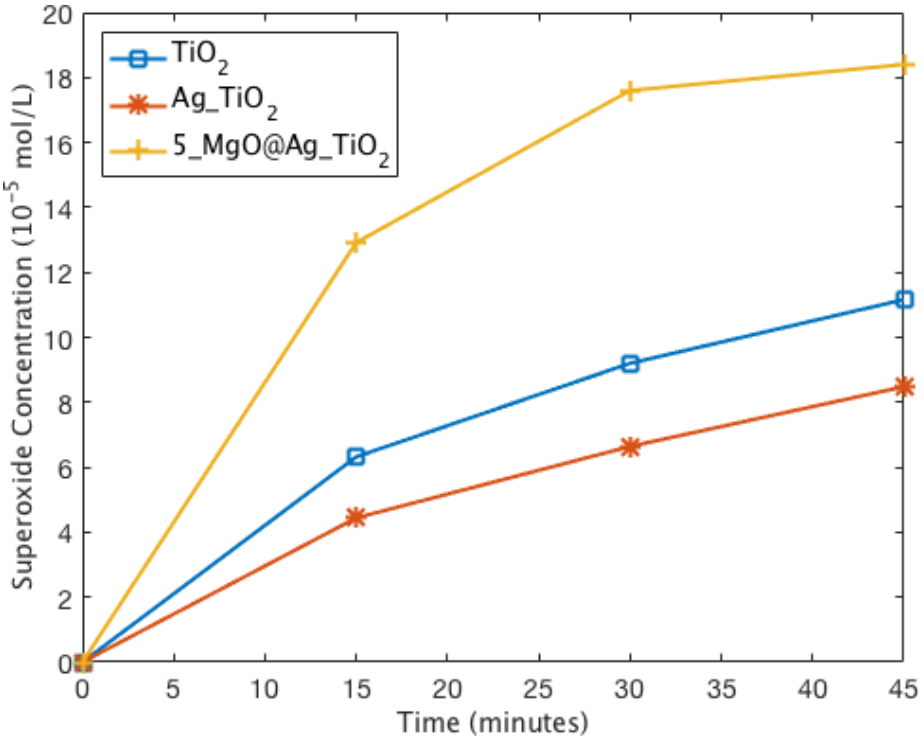

Figure 10: Superoxide production for TiO_2, Ag_TiO_2, and $5\_MgO@Ag\_TiO_2$

4.4 Proposed Reaction Mechanism

Based on the degradation and scavenger study results, reaction mechanisms for both Ag_TiO_2 and $5\_MgO@Ag\_TiO_2$ were developed and compared to one another. In Ag_TiO_2, incident light produces an electron-hole pair on TiO_2. The promoted electron travels to Ag, where it is trapped and may react with O_2 to form $\bullet O_2^-$. The hole remains on the surface of TiO_2, and may directly oxidize adsorbed phenol and its products, or react with H_2O to form •OH. Similarly, for $5\_MgO@Ag\_TiO_2$, incident radiation produces an electron-hole pair on TiO_2; the electron travels to Ag and then through the layer to Mg^{2+}, where it reacts with O_2 to form $\bullet O_2^-$. Due to its thin structure, the MgO layer is unlikely to hinder electron mobility, and the positive charge of Mg^{2+} as

compared to Ag^0 may be able to attract the electron to the catalyst surface (Zhao et al., 2017). In this case, the full pathway of the electron would be TiO_2 + hv → Ti^{3+} → Ag^0 → Mg^{2+}, from where it may react with O_2 to form $\bullet O_2^-$. The decreased •OH production along with near zero adsorption of phenol (Figure A3) together account for the decrease in mineralization performance demonstrated by 5_MgO@Ag_TiO_2, as both •OH and holes are known to be effective for phenol mineralization (Ilisz and Dombi, 1999; Wu et al., 2001). However, if •OH production is decreased, another radical is likely responsible for the degradation of phenol, and this may result from the increased $\bullet O_2^-$ production of 5_MgO@Ag_TiO_2. According to Equations 4.3-5, $\bullet O_2^-$ is able to react with a proton to form the hydroperoxyl radical, which may then react with phenol to abstract a proton and form H_2O_2. In this process, the phenoxy radical is formed, and through subsequent reactions with protons, electrons, and H_2O, the phenoxy radical may form a variety of intermediate compounds (Enache and Oliveira-Brett, 2011; Kozmér et al., 2014; Luzhkov, 2005; Sun et al., 2007).

$$\bullet O_2^- + H^+ \rightarrow HO_2^\bullet \tag{4.3}$$

$$HO_2^\bullet + PhOH \rightarrow H_2O_2 + C_6H_5O^\bullet \tag{4.4}$$

$$2H_2O_2 + h\nu \rightarrow 2H_2O + O_2 \tag{4.5}$$

However, although phenol is degraded in this reaction process, mineralization has not occurred; the phenol has only been converted into a variety of intermediate compounds, which accounts for the high degradation rate, but low mineralization rate of 5_MgO@Ag_TiO_2. To further evidence this theory, the degradation of phenol was tested with 0.3 mM H_2O_2 and no catalyst, under light and dark conditions. Shown in

Figure 11, without irradiation, almost no phenol is degraded or mineralized. Under solar irradiation, 76% of phenol is degraded, but only 8% is mineralized. These results support the proposed reaction mechanism in that when the solution is not irradiated, the H_2O_2 is not dissociated, and thus almost no $HO_2^{\bullet}$ is produced. Under irradiation, reactions following Equations 4.3-5 may occur, resulting in a high degradation and low mineralization of phenol.

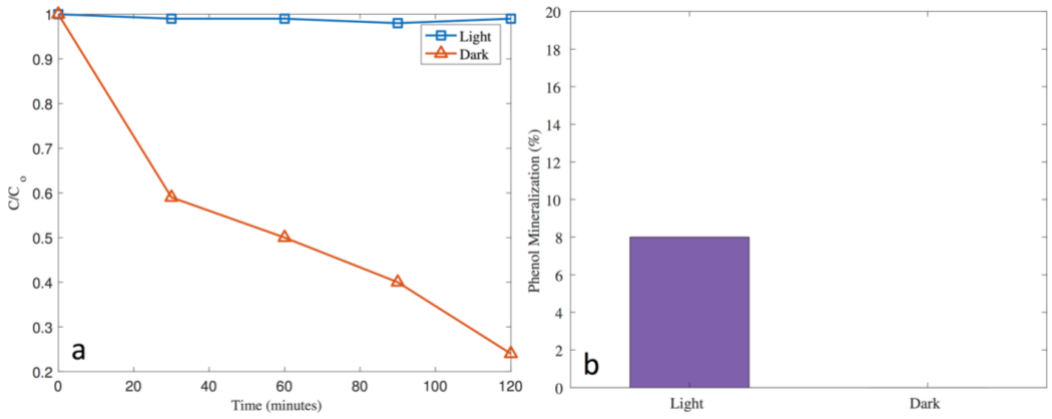

Figure 11: Phenol 120 min (a) degradation and (b) mineralization by the addition of 0.3mM H_2O_2

While 5_MgO@Ag_TiO_2 has low mineralization performance for phenol, its high production of $\bullet O_2^-$ makes it attractive for many other chemical processes. Polychlorinated biphenyls (PCBs) were once widely used as dielectric and coolant fluids, but their production was banned after their high environmental toxicity and persistence were identified. These compounds tend to accumulate as a result of their low aqueous solubility and may act as potent endocrine disruptors and carcinogens. While typical treatment methods such as sedimentation are costly with low effectiveness, $\bullet O_2^-$

has been shown effective to degrade many of these compounds completely within several hours (Hayyan et al., 2016). In addition, $\bullet O_2^-$ is effective to degrade hydrophobic compounds and nonaqueous-phase liquids for which •OH has low activity. Finally, $\bullet O_2^-$ may be used in various chemical and biological applications to produce a wide variety of compounds with high selectivity (Rastogi et al., 2009).

5. CONCLUSIONS

In summary, 5_MgO@Ag_TiO_2 has been synthesized by the growth of an ultrathin MgO layer on Ag decorated TiO_2 nanorods and demonstrates increased photoactivity as compared to uncoated samples. At the optimum coating thickness of 5 ALD cycles, $\bullet O_2^-$ production and light absorption are increased, while surface charge recombination is decreased by the passivation of existing defects. The increase in light absorption is attributed to additional light scattering induced by the MgO layer due to the difference in refractive indices of MgO and TiO_2, and this elevated absorption increases the generation of electron-hole pairs. As a result of the additional electron-hole pairs, reduced surface recombination, and reduced hole mobility by the MgO layer, $\bullet O_2^-$ production is increased. Under irradiation, $\bullet O_2^-$ may form $HO_2^\bullet$, which is effective to convert phenol in the phenoxy radical. ALD is thus shown to be an effective tool for engineering the surface properties of photocatalytic materials which may be used in the fields of water treatment and chemical production.

REFERENCES

Aarik J, Aidla A, Mändar H, Uustare T. Atomic layer deposition of titanium dioxide from TiCl4 and H2O: investigation of growth mechanism. Applied Surface Science 2001; 172: 148-158.

Bandara J, Pradeep UW. Tuning of the flat-band potentials of nanocrystalline TiO2 and SnO2 particles with an outer-shell MgO layer. Thin Solid Films 2008; 517: 952-956.

Beltrán FJ, Rivas FJ, Montero-de-Espinosa R. Mineralization improvement of phenol aqueous solutions through heterogeneous catalytic ozonation. Journal of Chemical Technology & Biotechnology 2003; 78: 1225-1233.

Benitez FJ, Beltran-Heredia J, Acero JL, Gonzalez T. Degradation of protocatechuic acid by two advanced oxidation processes: Ozone/UV radiation and H2O2UV radiation. Water Research 1996; 30: 1597-1604.

Buso D, Pacifico J, Martucci A, Mulvaney P. Gold-Nanoparticle-Doped TiO2 Semiconductor Thin Films: Optical Characterization. Advanced Functional Materials 2007; 17: 347-354.

Choi W, Termin A, Hoffmann MR. The Role of Metal Ion Dopants in Quantum-Sized TiO2: Correlation between Photoreactivity and Charge Carrier Recombination Dynamics. The Journal of Physical Chemistry 1994; 98: 13669-13679.

Cortés S, Sarasa J, Ormad P, Gracia R, Ovelleiro JL. Comparative Efficiency of the Systems O3/High pH And 03/catalyst for the Oxidation of Chlorobenzenes in Water. Ozone: Science & Engineering 2000; 22: 415-426.

Cozzoli PD, Comparelli R, Fanizza E, Curri ML, Agostiano A, Laub D. Photocatalytic Synthesis of Silver Nanoparticles Stabilized by TiO2 Nanorods: A Semiconductor/Metal Nanocomposite in Homogeneous Nonpolar Solution. Journal of the American Chemical Society 2004; 126: 3868-3879.

Cui Y, Ma Q, Deng X, Meng Q, Cheng X, Xie M, et al. Fabrication of Ag-Ag2O/reduced TiO2 nanophotocatalyst and its enhanced visible light driven

photocatalytic performance for degradation of diclofenac solution. Applied Catalysis B: Environmental 2017; 206: 136-145.

Elkanzi EM, Bee Kheng G. H2O2/UV degradation kinetics of isoprene in aqueous solution. Journal of Hazardous Materials 2000; 73: 55-62.

Enache TA, Oliveira-Brett AM. Phenol and para-substituted phenols electrochemical oxidation pathways. Journal of Electroanalytical Chemistry 2011; 655: 9-16.

Frank SN, Bard AJ. Heterogeneous photocatalytic oxidation of cyanide and sulfite in aqueous solutions at semiconductor powders. The Journal of Physical Chemistry 1977; 81: 1484-1488.

Fujishima A, Honda K. Electrochemical Photolysis of Water at a Semiconductor Electrode. Nature 1972; 238: 37-38.

Habisreutinger SN, Schmidt-Mende L, Stolarczyk JK. Photocatalytic Reduction of CO2 on TiO2 and Other Semiconductors. Angewandte Chemie International Edition 2013; 52: 7372-7408.

Hayyan M, Hashim MA, AlNashef IM. Superoxide Ion: Generation and Chemical Implications. Chemical Reviews 2016; 116: 3029-3085.

Herrmann J-M. Heterogeneous photocatalysis: fundamentals and applications to the removal of various types of aqueous pollutants. Catalysis Today 1999; 53: 115-129.

Hore S, Vetter C, Kern R, Smit H, Hinsch A. Influence of scattering layers on efficiency of dye-sensitized solar cells. Solar Energy Materials and Solar Cells 2006; 90: 1176-1188.

Ilisz I, Dombi A. Investigation of the photodecomposition of phenol in near-UV-irradiated aqueous TiO2 suspensions. II. Effect of charge-trapping species on product distribution. Applied Catalysis A: General 1999; 180: 35-45.

Irmak S, Erbatur O, Akgerman A. Degradation of 17β-estradiol and bisphenol A in aqueous medium by using ozone and ozone/UV techniques. Journal of Hazardous Materials 2005; 126: 54-62.

Ishibashi K-i, Fujishima A, Watanabe T, Hashimoto K. Detection of active oxidative species in TiO2 photocatalysis using the fluorescence technique. Electrochemistry Communications 2000; 2: 207-210.

Ji H, Chang F, Hu X, Qin W, Shen J. Photocatalytic degradation of 2,4,6-trichlorophenol over g-C3N4 under visible light irradiation. Chemical Engineering Journal 2013; 218: 183-190.

Kasprzyk-Hordern B, Ziółek M, Nawrocki J. Catalytic ozonation and methods of enhancing molecular ozone reactions in water treatment. Applied Catalysis B: Environmental 2003; 46: 639-669.

Kataoka K, Kijima N, Akimoto J. Ion-Exchange Synthesis, Crystal Structure, and Physical Properties of Hydrogen Titanium Oxide H2Ti3O7. Inorganic Chemistry 2013; 52: 13861-13864.

Kelly FM, Johnston JH. Colored and Functional Silver Nanoparticle−Wool Fiber Composites. ACS Applied Materials & Interfaces 2011; 3: 1083-1092.

Kozmér Z, Arany E, Alapi T, Takács E, Wojnárovits L, Dombi A. Determination of the rate constant of hydroperoxyl radical reaction with phenol. Radiation Physics and Chemistry 2014; 102: 135-138.

Kubacka A, Ferrer M, Martínez-Arias A, Fernández-García M. Ag promotion of TiO2-anatase disinfection capability: Study of Escherichia coli inactivation. Applied Catalysis B: Environmental 2008; 84: 87-93.

Le Formal F, Tetreault N, Cornuz M, Moehl T, Gratzel M, Sivula K. Passivating surface states on water splitting hematite photoanodes with alumina overlayers. Chemical Science 2011; 2: 737-743.

Lee K-C, Lin S-J, Lin C-H, Tsai C-S, Lu Y-J. Size effect of Ag nanoparticles on surface plasmon resonance. Surface and Coatings Technology 2008; 202: 5339-5342.

Li H, Wu X, Wang J, Gao Y, Li L, Shih K. Enhanced activity of AgMgOTiO2 catalyst for photocatalytic conversion of CO2 and H2O into CH4. International Journal of Hydrogen Energy 2016; 41: 8479-8488.

Li Q, Mahendra S, Lyon DY, Brunet L, Liga MV, Li D, et al. Antimicrobial nanomaterials for water disinfection and microbial control: Potential applications and implications. Water Research 2008; 42: 4591-4602.

Li TC, Góes MS, Fabregat-Santiago F, Bisquert J, Bueno PR, Prasittichai C, et al. Surface Passivation of Nanoporous TiO2 via Atomic Layer Deposition of ZrO2 for Solid-State Dye-Sensitized Solar Cell Applications. The Journal of Physical Chemistry C 2009; 113: 18385-18390.

Linsebigler AL, Lu G, Yates JT. Photocatalysis on TiO2 Surfaces: Principles, Mechanisms, and Selected Results. Chemical Reviews 1995; 95: 735-758.

Lipczynska-Kochany E. Degradation of aqueous nitrophenols and nitrobenzene by means of the Fenton reaction. Chemosphere 1991; 22: 529-536.

Liu L, Liu Z, Bai H, Sun DD. Concurrent filtration and solar photocatalytic disinfection/degradation using high-performance Ag/TiO2 nanofiber membrane. Water Research 2012; 46: 1101-1112.

Liu L, Pitts DT, Zhao H, Zhao C, Li Y. Silver-incorporated bicrystalline (anatase/brookite) TiO2 microspheres for CO2 photoreduction with water in the presence of methanol. Applied Catalysis A: General 2013; 467: 474-482.

Luzhkov VB. Mechanisms of antioxidant activity: The DFT study of hydrogen abstraction from phenol and toluene by the hydroperoxyl radical. Chemical Physics 2005; 314: 211-217.

Mali SS, Shim CS, Park HK, Heo J, Patil PS, Hong CK. Ultrathin Atomic Layer Deposited TiO2 for Surface Passivation of Hydrothermally Grown 1D TiO2 Nanorod Arrays for Efficient Solid-State Perovskite Solar Cells. Chemistry of Materials 2015; 27: 1541-1551.

Matthews RW. Photo-oxidation of organic material in aqueous suspensions of titanium dioxide. Water Research 1986; 20: 569-578.

Munter R. Advanced oxidation processes-current status and prospects. Vol 50, 2001.

Pérez-Estrada LA, Malato S, Gernjak W, Agüera A, Thurman EM, Ferrer I, et al. Photo-Fenton Degradation of Diclofenac: Identification of Main Intermediates and Degradation Pathway. Environmental Science & Technology 2005; 39: 8300-8306.

Peyton GR, Glaze WH. Destruction of pollutants in water with ozone in combination with ultraviolet radiation. 3. Photolysis of aqueous ozone. Environmental Science & Technology 1988; 22: 761-767.

Piwoński I, Spilarewicz-Stanek K, Kisielewska A, Kądzioła K, Cichomski M, Ginter J. Examination of Ostwald ripening in the photocatalytic growth of silver nanoparticles on titanium dioxide coatings. Applied Surface Science 2016; 373: 38-44.

Rajeshwar K, Chenthamarakshan CR, Goeringer S, Djukic M. Titania-based heterogeneous photocatalysis. Materials, mechanistic issues, and implications for environmental remediation. Pure and Applied Chemistry 2001; 73: 1849-1860.

Rastogi A, Al-Abed SR, Dionysiou DD. Sulfate radical-based ferrous–peroxymonosulfate oxidative system for PCBs degradation in aqueous and sediment systems. Applied Catalysis B: Environmental 2009; 85: 171-179.

Scheck CK, Frimmel FH. Degradation of phenol and salicylic acid by ultraviolet radiation/hydrogen peroxide/oxygen. Water Research 1995; 29: 2346-2352.

Schneider J, Matsuoka M, Takeuchi M, Zhang J, Horiuchi Y, Anpo M, et al. Understanding TiO2 Photocatalysis: Mechanisms and Materials. Chemical Reviews 2014; 114: 9919-9986.

Song J-G, Park J, Yoon J, Woo H, Ko K, Lee T, et al. Plasma enhanced atomic layer deposition of magnesium oxide as a passivation layer for enhanced

photoluminescence of ZnO nanowires. Journal of Luminescence 2014; 145: 307-311.

Sopyan I, Watanabe M, Murasawa S, Hashimoto K, Fujishima A. An efficient TiO2 thin-film photocatalyst: photocatalytic properties in gas-phase acetaldehyde degradation. Journal of Photochemistry and Photobiology A: Chemistry 1996; 98: 79-86.

Sun Y, Wu J, Liu C. A comparison of transition state of phenol in H-atom abstraction by methyl and methylperoxyl radicals. Chinese Science Bulletin 2007; 52: 1182-1186.

Tekin H, Bilkay O, Ataberk SS, Balta TH, Ceribasi IH, Sanin FD, et al. Use of Fenton oxidation to improve the biodegradability of a pharmaceutical wastewater. Journal of Hazardous Materials 2006; 136: 258-265.

Tian Y, Tatsuma T. Plasmon-induced photoelectrochemistry at metal nanoparticles supported on nanoporous TiO2. Chemical Communications 2004: 1810-1811.

Trapido M, Veressinina Y, Munter R. Advanced Oxidation Processes for Degradation of 2,4-Dichlo- and 2,4-Dimethylphenol. Journal of Environmental Engineering 1998; 124: 690-694.

Upelaar GF, Meijers RT, Hopman R, Kruithof JC. Oxidation of Herbicides in Groundwater by the Fenton Process: A Realistic Alternative for O3/H2O2 Treatment? Ozone: Science & Engineering 2000; 22: 607-616.

Vasilopoulou M, Georgiadou DG, Soultati A, Boukos N, Gardelis S, Palilis LC, et al. Atomic-Layer-Deposited Aluminum and Zirconium Oxides for Surface Passivation of TiO2 in High-Efficiency Organic Photovoltaics. Advanced Energy Materials 2014; 4: 1400214-n/a.

Verbruggen SW. TiO2 photocatalysis for the degradation of pollutants in gas phase: From morphological design to plasmonic enhancement. Journal of Photochemistry and Photobiology C: Photochemistry Reviews 2015; 24: 64-82.

Wu C, Liu X, Wei D, Fan J, Wang L. Photosonochemical degradation of Phenol in water. Water Research 2001; 35: 3927-3933.

Wu K, Xie Y, Zhao J, Hidaka H. Photo-Fenton degradation of a dye under visible light irradiation. Journal of Molecular Catalysis A: Chemical 1999; 144: 77-84.

Xi L, Chiam SY, Mak WF, Tran PD, Barber J, Loo SCJ, et al. A novel strategy for surface treatment on hematite photoanode for efficient water oxidation. Chemical Science 2013; 4: 164-169.

Xiao F-X, Miao J, Tao HB, Hung S-F, Wang H-Y, Yang HB, et al. One-Dimensional Hybrid Nanostructures for Heterogeneous Photocatalysis and Photoelectrocatalysis. Small 2015; 11: 2115-2131.

Xu X, Duan X, Yi Z, Zhou Z, Fan X, Wang Y. Photocatalytic production of superoxide ion in the aqueous suspensions of two kinds of ZnO under simulated solar light. Catalysis Communications 2010; 12: 169-172.

Yasmina M, Mourad K, Mohammed SH, Khaoula C. Treatment Heterogeneous Photocatalysis; Factors Influencing the Photocatalytic Degradation by TiO2. Energy Procedia 2014; 50: 559-566.

Yu J, Xiong J, Cheng B, Liu S. Fabrication and characterization of Ag–TiO2 multiphase nanocomposite thin films with enhanced photocatalytic activity. Applied Catalysis B: Environmental 2005; 60: 211-221.

Yuan Z-Y, Su B-L. Titanium oxide nanotubes, nanofibers and nanowires. Colloids and Surfaces A: Physicochemical and Engineering Aspects 2004; 241: 173-183.

Zhao H, Chen J, Rao G, Deng W, Li Y. Enhancing photocatalytic CO2 reduction by coating an ultrathin Al2O3 layer on oxygen deficient TiO2 nanorods through atomic layer deposition. Applied Surface Science 2017; 404: 49-56.

APPENDIX

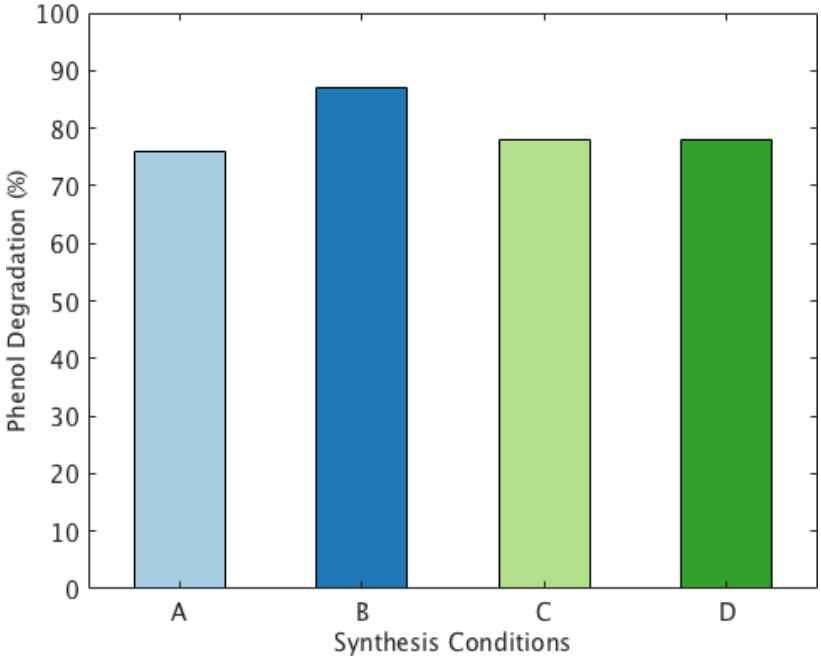

Figure A1: Optimal Ag deposition irradiation time

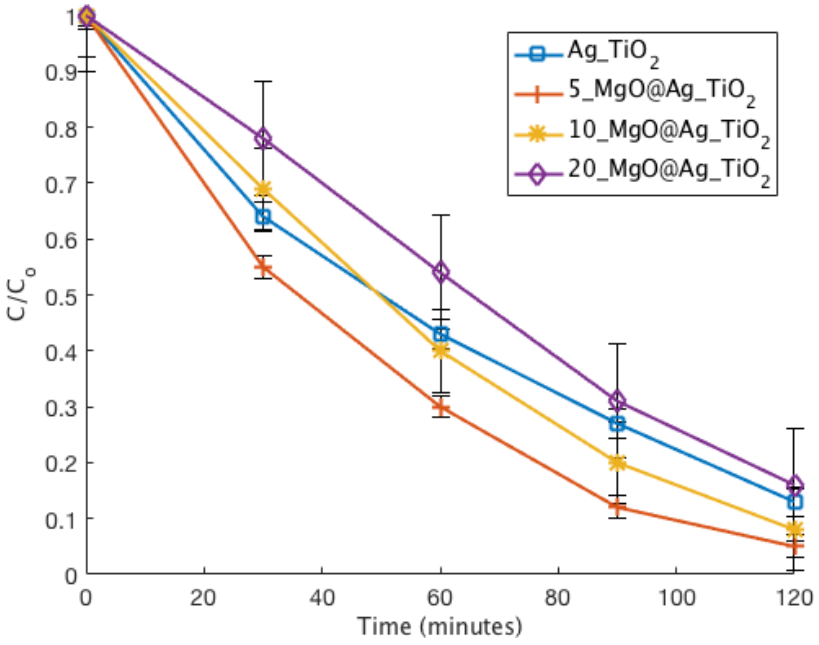

Figure A2: Effect of number of MgO cycles on phenol degradation for varying irradiation times

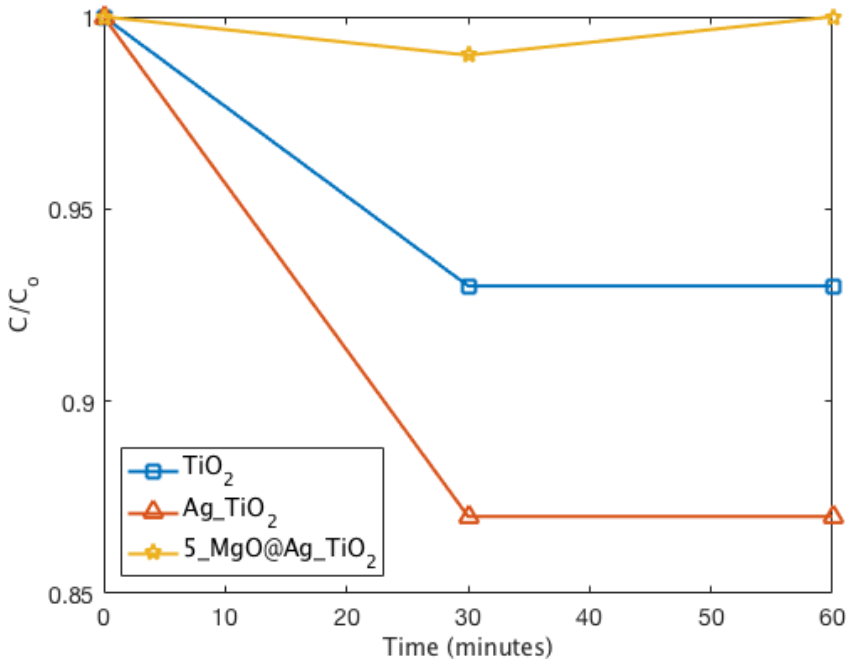

Figure A3: Adsorption equilibrium of phenol for TiO_2, Ag_TiO_2, and $5\_MgO@Ag\_TiO_2$

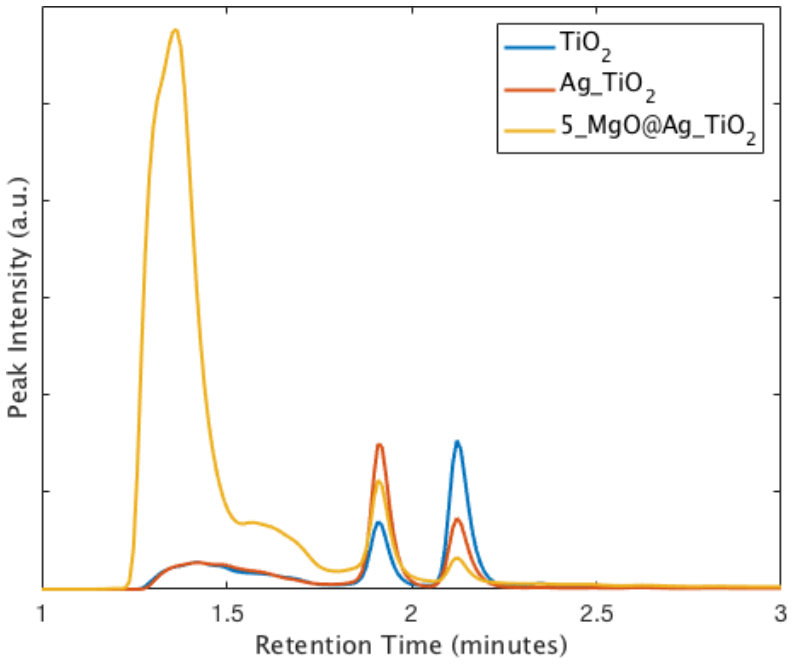

Figure A4: HPLC Spectra for TiO_2, Ag_TiO_2, and 5_MgO@AgTiO_2 after 120 minutes irradiation

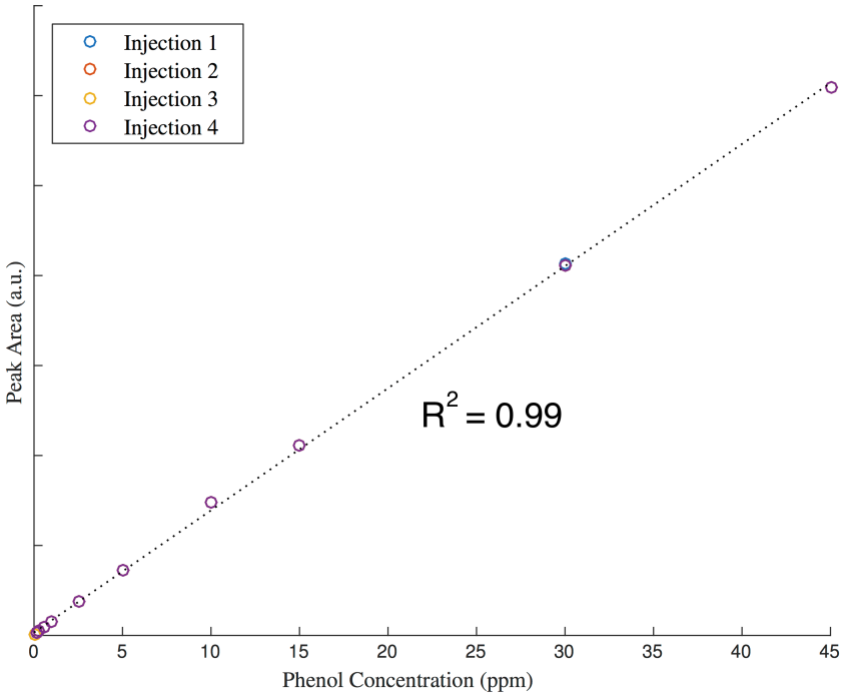

Figure A5: HPLC phenol calibration from 0.015-45 ppm, four separate injections per concentration level

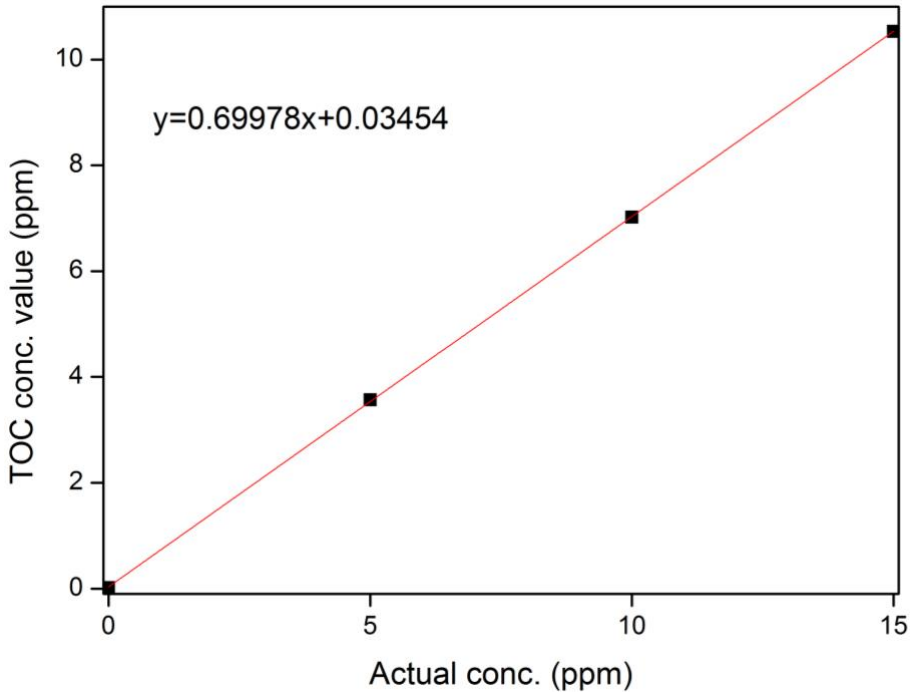

Figure A6: TOC concentration vs phenol concentration

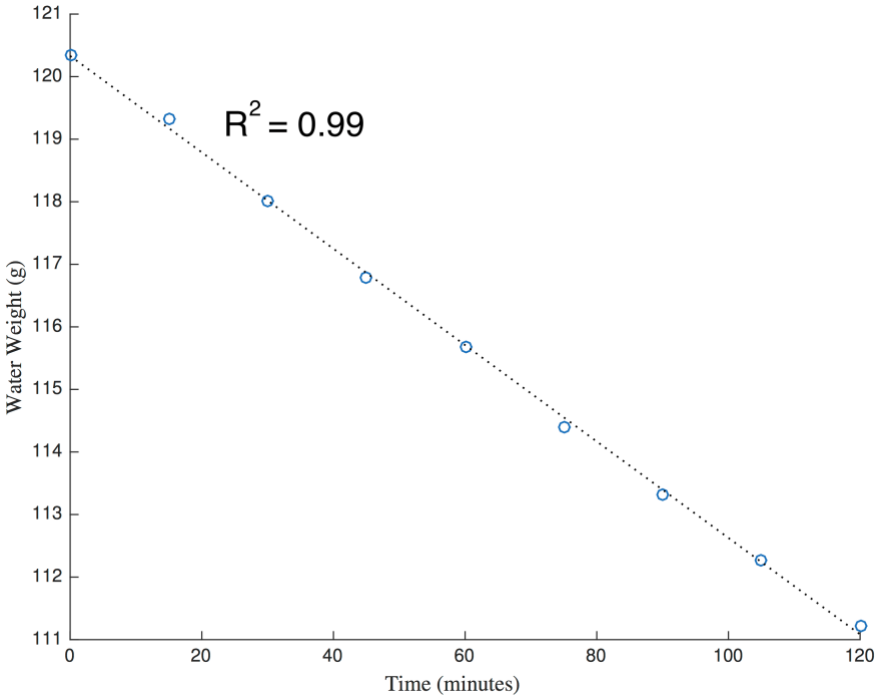

Figure A7: Water evaporation rate by cooling fan